2011

Measurement of White Matter Structure Changes in Amyotrophic Lateral Sclerosis Using Fractal Analysis

Zao Liu
Cleveland State University

MEASUREMENT OF WHITE MATTER STRUCTURE CHANGES IN AMYOTROPHIC LATERAL SCLEROSIS USING FRACTAL ANALYSIS

ZAO LIU

Bachelor of Engineering in Biomedical Engineering

Southeast University

May 2009

Submitted in partial fulfillment of requirements for the degree

MASTER OF SCIENCE IN BIOMEDICAL ENGINEERING

at the

CLEVELAND STATE UNIVERSITY

August 2011

This Thesis has been approved
for the Department of CHEMICAL AND BIOMEDICAL ENGINEERING
and the College of Graduate Studies by

Thesis/Dissertation Chairperson, Guang H. Yue, Ph.D

Department of Chemical and Biomedical Engineering

Department & Date

Nolan B. Holland, Ph.D

Department of Chemical and Biomedical Engineering

Department & Date

R. Jeffery Dean, Ph.D

Dept. of Biological, Geological and Environmental Sciences

Department & Date

Sridhar Ungarala, Ph.D

Department of Chemical and Biomedical Engineering

Department & Date

ACKNOWLEDGEMENTS

First I would express my deepest gratitude to my advisor, Dr. Guang H. Yue for his great guidance. He always supports me when I come up with any new idea. This is so important, otherwise there is no this thesis at all. His sincere and strict attitude to research work impressed me and will continuously impact me in the future, which is same precious as scientific knowledge he taught me.

Second, I would like to thank my committee members, Dr. Nolan B. Holland, Dr. R. Jeffery Dean, and Dr. Sridhar Ungarala for their critical suggestion and advice during this research work. I really appreciate your effort and time to make this work done.

Third, I would like to acknowledge my parents, Mingxin Liu, and Huazhen Wang. They are always behind me no matter what happened.

My final acknowledgement goes to Becky Laird and Darlene G. Montgomery. Thank you for your support all the time during this research work.

MEASUREMENT OF WHITE MATTER STRUCTURE CHANGES IN AMYOTROPHIC LATERAL SCLEROSIS USING FRACTAL ANALYSIS

ZAO LIU

ABSTRACT

Amyotrophic lateral sclerosis (ALS) is recognized as a motor neuron disorder affecting the structure and function of the brain and neuromuscular system. Very little is known, however, that the nervous system degeneration is dependent on disease phenotypes of ALS. The purpose of this study was to determine the degree of brain white matter (WM) structure degeneration in four ALS patient groups characterized by their clinical signs and neuroimaging measurements. Fractal dimension (FD) of three-dimensional (3D) brain WM images was quantitatively analyzed to evaluate the WM structural complexity, including complexity levels of the WM skeleton, surface and general structures in ALS patients and control subjects. A total of 100 participants were assigned into five groups: ALS patients with frontotemporal dementia (ALS-FTD, n=20), ALS patients with predominantly upper motor neuron (UMN) signs and hyperintensity MRI signals on corticospinal tract (CST) (UMN-CST^{+}, n=20), ALS patients with predominantly UMN signs but without hyperintensity signal on CST (UMN-CST-, n=27), ALS patients with an equal amount of UMN and lower motor neuron (LMN) signs (ALS-classic, n=22), and a neurological control group (n=11). The brain was extracted

from head images by using the FSL package, and the WM was segmented from and the brain images before being separate into WM images of the left and right hemispheres. Subsequently, skeletons of the WM bundles were obtained using a 3-dimensional thinning method. FD analysis was applied onto three forms of the WM structure: skeleton, surface, and general structure. FD of the skeletons and general structure in ALS-FTD patients was significantly smaller ($P<0.05$ – $P<0.01$) than the controls and UMN-CST^{+}, and ALS-classic patients. The FD of UMN-CST^{+} patients was significantly larger ($P<0.05$ – $P<0.01$) than UMN-CST^{-} and ALS-classic patients. These results suggest that the complexity level of brain WM network is dependent on ALS disease phenotypes and ALS patients with dementia suffer the worst brain WM structural degeneration. Asymmetry of WM structure complexity between left and right hemispheres was observed in ALS-FTD and ALS-classic patients. Analysis of the whole brain WM structure was more sensitive than that of either of the hemispheres with the skeleton being the most sensitive structure for detecting degenerative changes. These findings provided new information in better understanding ALS disease progression in the central nervous system and for seeking effective treatments of this devastating disease.

Key Words: Amyotrophic lateral sclerosis (ALS), degeneration, white matter (WM), fractal dimension (FD), skeleton, surface, general structure, magnetic resonance imaging (MRI).

TABLE OF CONTENTS

LIST OF TABLES

LIST OF FIGURES

LIST OF ABBREVIATIONS

2D = Two dimensional

3D = Three dimensional

ALS = Amyotrophic lateral sclerosis

ANOVA = Analysis of variance

BET = Brain extraction tool

CNS = Central nervous system

CSF = Corticospinal fluid

CST = Corticospinal tract

CT = Computed tomography

DTI = Diffusion tensor imaging

FA = Fractional anisotropy

FAST = FMRIB's automated segmentation tool

FD = Fractal dimension

FLIRT = FMRIB's linear image registration tool

FMRIB = Functional magnetic resonance imaging of the brain

FSL = FMRIB software library

FTD = Frontotemporal dementia

GM = Grey matter

HarFA = Harmonic and fractal imaging analyzer

LMNs = Lower motor neurons

MNI = Montreal neurological institute

MRI = Magnetic resonance imaging

PNS = Peripheral nervous system

UMNs = Upper motor neurons

WM = White matter

CHAPTER I

INTRODUCTION AND BACKGROUND

1.1. Amyotrophic Lateral Sclerosis (ALS)

1.1.1. Introduction

Amyotrophic lateral sclerosis (ALS) is a progressive neurodegenerative disease that affects both upper motor neurons (UMNs) and lower motor neurons (LMNs). Although the cause of ALS and related neural degeneration are not well understood, past studies have shown that ALS patients suffer from behavioral dysfunction (Olney et al., 2005), and some of them have cognitive impairment (Phukan et al., 2007) and encounter depression and anxiety (Lou et al., 2003). Patients afflicted by ALS usually die within five years mainly as a result of dysfunction of the respiratory system. This cruel disease was first described by the French neurologist Jean-Martin Charcot in 1869 and did not receive much national or international attention until Lou Gehrig, a star baseball player with the New York Yankees, died of ALS in 1936. Therefore, ALS is also referred to as "Lou Gehrig's Disease". The disease is relatively rare, occurring in only 2 of 100,000

people each year (Logroscino et al., 2010). Currently, about 30,000 Americans have been diagnosed with ALS, typically between the ages of 40and 70.

The name of Amyotrophic lateral sclerosis indicates that it is a neuron disease with both upper and lower motor neuron signs. The Amyotrophic comes from the Greek language, in which the A refers to no, the Myo means muscle and the Trophic identifies nourishment. In whole, amyotrophic means no muscle nourishment and refers to muscle atrophy, weakness, cramp and fasciculation, which are the signs of lower motor neuron disease. The Lateral represents the areas in spinal cord where locates the nerve cells innervate the muscles. When the lateral region degenerates, scarring or hardening, referred to as Sclerosis, will occur (Rowland et al., 2001).

1.1.2. Motor Neuron Degeneration in ALS

The motor neurons provide control signals to skeletal muscles for voluntary movements and muscle power. The degenerated motor neuron in ALS can no longer send normal action potentials to muscle fibers innervated by the motor neurons. Consequently, the corresponding muscle contractions are disrupted and the muscle atrophies, leading to motor function disability. The degeneration of UMNs arises in the cerebral cortex, while the degeneration of LMNs arises in the brainstem and spinal cord (Mitusmoto et al., 1998).

Although the exact cause of ALS is still unknown, some emerging clues suggest that excitotoxicity plays a critical role by damaging the motor neurons. It has been reported that Glutamate (a potentially neuroexcitotoxic compound and neural transmitter of the corticospinal system and certain spinal cord interneurons) is conformed to link with the defect in the transport system in ALS patients (Plaitakis et al., 1987). To inhibit

presynaptic release of glutamate, riluzole was first developed as an antiepileptic drug to deal with ALS. However, riluzole canonly slow the course of ALS, whilst the long-term ALS outcome is still the same.

1.2. Neuroanatomy

1.2.1. Neuron

Neurons are the main signaling units of the nervous system (Kandel et al., 2000). Their functions are to sense any changes in environment, communicate those changes to other neurons, and command body's response to those sensations. A neuron consists of a soma (cell body) and neuritis (axon and dendrites). The axons are wrapped in a sheath of insulating lipoprotein called myelin to increase the signal conduction speed.

1.2.1.1. Upper Motor Neuron (UMN)

Upper motor neurons start in the motor cortex of brain (primarily in layer V of the precentral gyrus) and terminate within the medulla or within the spinal cord (Figure 1.1); they carry motor information down to the spinal cord, but they do not initiate the target muscle directly. Betz cells are the main neurons for voluntary movement and are located within layer V of the primary motor cortex, the internal pyramidal layer of the precentral gyrus. These UMNs send long axons to the contralateral motor nuclei of the cranial nerves (the lower motor neurons in the brain stem) and to the spinal nerves (the lower motor neurons in the ventral horn of the spinal cord). These axons form the corticospinal tract (CST).

1.2.1.2. Lower Motor Neuron (LMN)

LMNs are the motor neurons that connect the brainstem and spinal cord to the muscle fibers that transfer the nerve impulses from the upper motor neurons to the

muscles (Figure 1).

Lower motor neurons in the spinal cord innervate limb and body muscles and lie in the ventral horn of the spinal cord. The axons these motor neurons bundle together to form ventral roots, which join with a dorsal root to form a spinal nerve exiting the cord through the notches between vertebrae. The motor neurons that project fibers to one spinal nerve are said to belong to a spinal segment. The segments are named after the vertebra where the nerve originates: cervical segments, thoracic segments, lumbar segments, and sacral segments. Motor neurons located in different segments innervate muscles in different body parts. For instance, spinal cord cervical segments contain the motor neurons that innervate arm muscles, whilst spinal cord lumbar segments contain the neurons that innervate leg muscles.

LMNs could be classified as alpha motor neurons and gamma motor neurons according to the types of muscles which they innervate: Alpha motor neurons control extrafusal muscle fibers, which are the most numerous type of muscle fiber and involved in making joint movements. Gamma motor neurons control intrafusal muscle fibers, which compose muscle spindles with sensory afferents indicating changes of muscle length.

Alpha motor neurons generate and send control pulses to connected muscles that in turn, make contraction and produce force and movement. Each alpha motor neuron connects with a given number of muscle fibers through the motor axon. Sir Sherrington, a well-known neurophysiologist and one of two Nobel Prize winners in physiology and Medicine in 1932, termed this functional unit (motor neuron, its axon and all the innervated muscle fibers) as a motor unit. The collection of all the alpha motor neurons

that innervate one specific single muscle is called a motor neuron pool; all the muscle contractions for this muscle are controlled by the individual or series of action potentials from this motor neuron pool. To summarize, a motor unit contains an alpha motor neuron, its axon and all muscle fibers it innervates; a motor neuron pool consists of all the alpha motor neurons that innervate one single muscle.

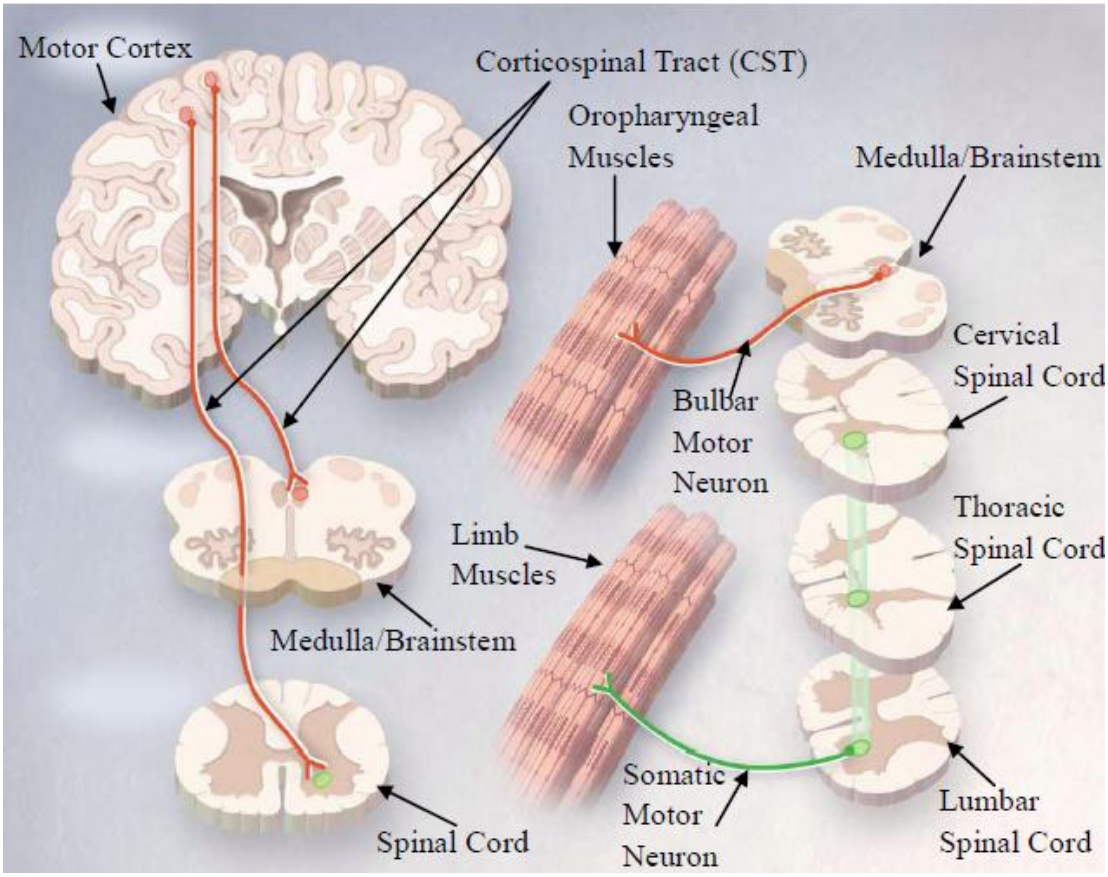

Figure 1: UMN-CST-LMN neuron system. UMNs send long axons (CST) to the contralateral motor nuclei of the cranial nerves (LMNs in the brain stem) and to the spinal nerves (LMNs in the ventral horn of the spinal cord). (Rowland et al., 2001 with modified)

1.2.2. Corticospinal Tract (CST)

The brain communicates with the lower motor neurons in the spinal cord through the axons descending from the brain to the spinal cord (Figure 1.1). Those axons form two groups of pathways: lateral pathways, which are involved in voluntary movement of

the distal musculature and are under direct cortical control; and ventromedial pathways, which are involved in the control of posture and locomotion and are under both the brain and brain stem control. The CST is the most important component of the lateral pathways, which connects the UMNs and LMNs. Two-thirds of the axons in the CST start in areas 4 (primary motor cortex) and 6 (premotor and supplementary motor cortices) of the frontal lobe, whilst most of the remaining axons derive from the somatosensory areas of the parietal lobe and serve to regulate the flow of somatosensory information to the brain (Bear et al., 2001).

Axons of the CST originating from the cortex pass through the internal capsule (bridging the telencephalon and thalamus), the base of the cerebral peduncle (a large collection of axons in the midbrain), the pons, and then collectively to form a tract at the base of the medulla. Figure 2 shows the DTI of CST in three evaluated levels: the corona radiate, the internal capsule, and the pons. The CST is consisted of two separate tracts in the spinal cord: the lateral CST and anterior CST. Approximately 80% of the CST fibers cross over to the contralateral side in the medulla oblongata (pyramidal decussation), traveling in the lateral CST; ~10% of the fibers enter the lateral CST on the same side; and the remaining 10% of the fibers cross over at the level that they exit the spinal cord, traveling in the anterior corticospinal tract.

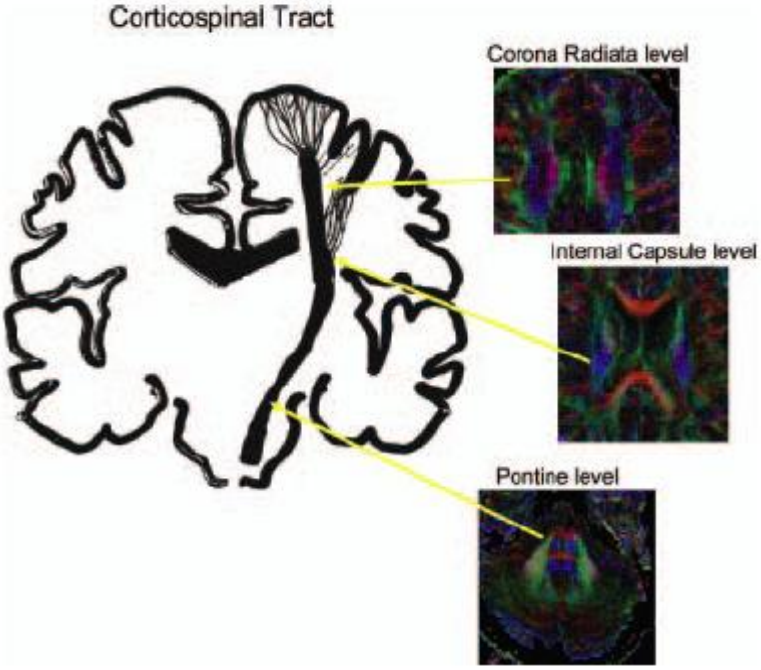

Figure 2: MR diffusion tensor imaging (DTI) of the three evaluated levels of the cortiocpinal tract: (i) corona radiate, (ii) internal capsule, and (iii) pons. Corticospinal tract is marked with blue in each level. (Karlsborg et al., 2004)

1.2.3. White Matter (WM)

The white matter (WM) is one of the two most important components of the central nervous system and consists mostly of myelinated axons, compared with gray matter (GM), which contains cell bodies of neurons. It is white because the outer layer (myelin) is a fatty substance. WM as a tissue functions primarily with conducting impulses from one population of neurons (grey matter [GM]) to another. The CST is part of the WM system that caries information from GM of sensorimotor areas in the cerebral cortex to motor neurons in the brain stem and spinal cord.

There are three different tracts contained in the WM system: (i) projection tracts,

which send impulses from the cortex to other brain regions, and to nuclei in brain stem and spinal cord, or from sensory receptor to the brain; (ii) commissural tracts, which pass action potentials between left and right hemispheres of the brain through commissures; and (iii) association tracts, which carry information between lobes within a single hemisphere. The CST belongs to the projection tracts.

1.3. White Matter in ALS

1.3.1. Overview

At a microscopic level, ALS is demonstrated by axonal swelling with neurofilament accumulations, axonal Wallerian degeneration and dendrites attenuation (Cluskey and Ramsden, 2001). At a macroscopic level, the changes reflect the microscopic changes indeed, such as axon degeneration (Metwalli et al., 2010) and demyeliniztion.

1.3.2. Imaging of White Matter Changes in ALS

The diagnosis of ALS requires the presence of both UMN degeneration signs (weakness, wasting and fasciculation) and LMN degeneration signs (increased or clonic tendon reflexes, spasticity, pseudobulbar features, Hoffmann reflex and extensor plantar response). To provide reliable criteria for ALS diagnosis, the E1 Escorial Criteria for therapeutic trials were developed by medical and research experts in ALS associated with the World Federation of Neurology (Brooks et al., 2000). However, the criteria are considered too restrictive; some patients presumably died from ALS are not diagnosed as an ALS patient. Genetic testing is not a routine evaluation unless there is a family history of ALS.

Magnetic Resonance Imaging (MRI) is an ideal method for diagnosis of UMN signs because it is noninvasive and can provide different contrasts between different tissues, which could detect the abnormities in ALS that could not be detected by other devices, such as computed tomography (CT) (Mitusmoto et al., 1998). One previously used MRI technique for detecting UMN abnormalities in ALS is measurement of image signal intensity of the CST. Abnormal bilateral hyperintensity in the posterior portion of the posterior limb of CST in the internal capsule in T2-weighted image was demonstrated to relate to the degeneration of CST (Yagishita et al., 1994). Other MRI approaches, such as evaluation of global cerebral atrophy both in motor and extra-motor areas using T1-weighted images (Kassubek et al., 2005) and estimating WM integrity using diffusion tensor imaging (DTI) (Graham et al., 2004) have been reported to be useful as quantitative tools for monitoring progression of UMN pathology in longitudinal studies.

1.4. Skeleton

The concept of skeleton was introduced by Blum in 1967. Skeleton, also called topological skeleton, is the thin version of object that is equidistant to its boundaries. In other words, skeleton is the medial axis of that object. It defines an object geometrically, summarizes the topological properties (connectivity, topology, size, shape and orientation) of that object, and reserves all the information needed to reconstruct the original object. In a two-dimensional brain image, skeleton is the one-pixel width central line within a WM fiber bundle; in a three-dimensional brain image, it is a one-voxel width central line within the fiber bundle. In this research, skeletons were extracted from brain WM structures in ALS patients and control subjects because the medial axis can preserve the

topological properties and the connectivity of the WM tracts/fiber bundles. Physiologically, extracted skeletons represent complexity of the WM connectivity network, such as fiber crossings and bifurcations. The method used for extracting WM skeletons and their analysis has previously been described (Zhang et al. 2005). Brain WM skeleton, surface (reflecting WM surface convolution), and general structure (showing entire shape of the WM structure) were three forms of the WM structure evaluated in this study.

1.5. Fractal Dimension

1.5.1. Fraction Dimension Definition

Dimension is the number of variables in a dynamic system. In Euclidean space, there are three dimensions: D=1, D=2, and D=3.

Fractal Dimension is also called Hausdorff Dimension, which accurately measures the dimension of irregular geometric objects, for example fractals.

In the Euclidean space, amplifying a one-dimensional line twice will obtain two identical line segments; four identical squares are seen if a two-dimensional square is amplified by two; eight three-dimensional cubes are obtained with the magnification of two. Figure 3 demonstrates the magnification procedure.

According to the examples mentioned above, the relationship between the magnification and dimension could be express by the Eq.1.1.

$$e^D = N \tag{1.1}$$

In this equation, e is magnification, N is number of copies, and D is dimension. The dimension could be obtained by taking the natural logarithm of both sides of Eq.1.1 as Eq.1.2.

$$D = \frac{\ln N}{\ln e} \tag{1.2}$$

Both Eq.1.1 and Eq.1.2 could also be applied to Fraction Dimension.

1.5.2. Measurement of Fractal Dimension

There are several methods to calculating FD, such as the box-counting method, the correlation dimension method, etc. When estimating the image FD, the box-counting method is preferred, because it can apply on the target with or without self-similarity. It works by repeatedly covering the different-sized box (r) onto the fractal and counting the number of boxes (N) needed to completely cover the fractal (Figure 4A, B). In Figure 4, two meshes with different sized box (5-pixel and 15-pixel) were overlaid onto a two-dimensional (2D) WM binary image. For these two meshes, 1286 5-pixel-boxes (Figure 4A) and 197 15-pixel-boxes (Figure 4B) covered all the WM structure completely.

The FD could be defined in the power-law relationship (Eq.1.3)

$$N = kr^{-FD} \tag{1.3}$$

The FD was obtained by linear fitting the Eq.1.4.

$$\ln N = FD \ln \frac{1}{r} + \ln k \tag{1.4}$$

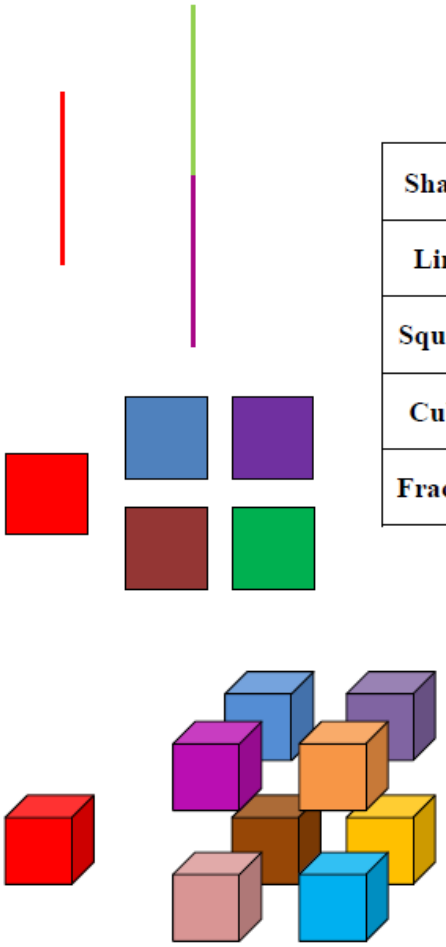

Shape	Dimension	No. of identical shapes
Line	1	2^1
Square	2	2^2
Cube	3	2^3
Fractal	D	2^D

Figure 3: Illustration of relationship between dimension and magnification

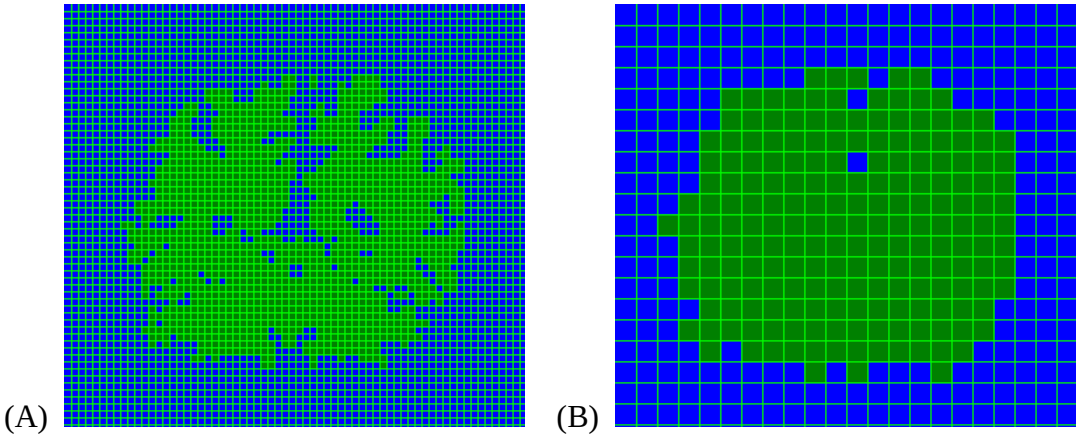

Figure 4: Traditional 2D box-counting method, covering a 2D sample of binary WM slice with mesh with different box sizes (*r*) and the number of boxes (*N*) needed to cover the whole WM structure completely (green boxes in the images).
(A) r=5, N=1286 and (B) r=15, N=197. The images were generated by the box-counting package from HarFA (http://www.fch.vutbr.cz/lectures/imagesci/) using data from one subject.

1.5.3. Fractal Dimension Analysis Applied to Understand Brain WM Structure

Fractal dimension (FD) method is a promising method to evaluate condition of the brain structure because it is not only sensitive in detecting brain WM degeneration in normal aging, but also can notice the WM abnormalities due to pathological reasons.

Zhang et al. used FD to estimate age and gender effects on brain WM structure complexity in healthy human subjects and found that the WM structural complexity decreased with aging and this kind of deterioration is not uniformly distributed between genders or across brain hemispheres (Zhang et al., 2007). The FD method was applied to analysis of brain structures in multiple sclerosis (MS); significant changes of white matter structure were identified (Francisco et al., 2007) along with abnormal morphology of GM early in the course of MS disease (Francisco et al., 2009).

1.6. Thesis Objective and Organization

1.6.1. Rationale

It is well accepted that ALS is caused by structural and functional degenerations at both UMN and LMN levels. However, findings from previous research on this topic were not consistent, sometimes even contradictory. One potential reason for this could be that adaptations to ALS are dependent on disease phenotypes; one type of ALS may affect the system more severely than the other. If this is true, investigating all types of ALS patients as one condition may only yield minimal to moderate levels of alteration in the hypothesized direction. Therefore, the major goal of this research was to evaluate brain WM structural degeneration in four types of ALS patients classified on their clinical signs and MRI diagnostic features. It was hypothesized that the degree of brain WM

degeneration in ALS would depend on the disease type.

1.6.2. Objective

The overall objective of this thesis was to apply FD analysis to understand morphological adaptations of brain WM structure afflicted by ALS. Specifically, a large group of ALS patients were categorized into four subgroups according to the clinical symptoms and conventional MRI results; the degree of WM degeneration was assessed in each of and compared among the four ALS patient groups. Three dimensional (3D) FD analysis was performed to understand three forms of brain WM structures in ALS: skeleton - interior structure, surface - interface structure between GM and WM, and general structure – the entire shape of WM (it partly reflects the volume of WM). The combination of these three forms structural analyses in classified ALS groups provided a comprehensive characterization of brain WM structural adaptations caused by different ALS phenotypes.

1.6.3. Specific Aims

Aim 1 – To evaluate FD of brain WM structure to determine its complexity level and compare the WM structural complexity among four groups of ALS patients.

Hypothesis 1 – The level of the WM structural complexity would be the lowest in ALS patients with dementia.

Aim 2 – To compare FD values among three forms of brain WM structure, skeleton, surface and general structure.

Hypothesis 2 – FD measurement of the skeleton would be the most sensitive variable among the three in detecting brain WM degeneration in a given ALS patient group.

Aim 3 – To determine whether the complexity level of brain WM structure was symmetrical between left and right hemispheres and whether assessing the whole brain was more sensitive in detecting the WM structure degeneration than analyzing each individual hemisphere.

Hypothesis 3 – The level of brain WM structural complexity would be asymmetrical in some type of ALS patients but not all; FD measurement of the whole brain WM would be more sensitive than that of each individual hemisphere in finding significant brain WM structural changes.

1.6.4. Thesis Organization

Chapter 1: Introduction and Background

This chapter introduces general background of the nervous system and ALS; provides an overview of neuroanatomy, especially WM anatomy; and describes concepts of skeleton and fractal dimension. The overall objective and specific aims, and organization of the thesis are stated at the end of the chapter.

Chapter 2: Materials and Methods

This chapter explains the study subjects and classification of ALS subgroups; MRI data (image) acquisition; and image processing, WM extraction and FD analysis.

Chapter 3: Results

This chapter reports FD (WM structure complexity) comparison results among ALS subgroups and between ALS and healthy controls within same hemispheres, between two hemispheres, and in the whole brain.

Chapter 4: Discussion

This chapter discusses main findings of this research, points future directions, and

acknowledges limitations of the current study.

1.7. Reference

Bear MF, Connors BW, Paradiso MA. Neuroscience: exploring the brain. Philadeplhia: Lippincott Williams & Wilkins, 2001.

Brooks BR. E1 Escorial revisited: revised criteria for the diagnosis of amyotrophic lateral sclerosis. Amyotroph Lateral Scler Other Motor Neuron Disord 2000; 1:293-299.

Cluskey S, Ramsden DB. Mechanisms of neurodegeneration in amyotrophic lateral sclerosis. J Clin Pathol: Mol Pathol 2001; 54:386-392.

Francisco J. Fractal dimension analysis of grey matter in multiple sclerosis. Journal of the Neurological Sciences 2009; 282:67-71.

Francisco J. Fractal dimension and white matter changes in multiple sclerosis. NeuroImage 2007; 36:543-549.

Graham JM. Diffusion tensor imaging for the assessment of upper motor neuron integrity in ALS. Neurology 2004; 63:2111-2119.

Kandel ER, Schwartz JH, Jessell TM. Principles of neural science. New York: McGraw-Hill, Health professions Division, 2000.

Karlsborg M. Corticospinal tract degeneration and possible pathogenesis in ALS evaluated by MR diffusion tensor imaging. ALS and other motor neuron disorders 2004; 5:136-140.

Kassubek J. Global brain atrophy and corticospinal tract alterations in ALS, as investigated by voxel-based morphometry of 3-D MRI. Amyotrophic Lateral Sclerosis 2005; 6:213-220.

Logroscino G. Incidence of amyotrophic lateral sclerosis in Europe. J Neurol Neurosurg Psychiatry 2010; 81:385-90.

Lou J. Fatigue and depression are associated with poor quality of life in ALS. Neurology 2003; 60:122-3.

Metwalli NS. Utility of axial and radial diffusivity from diffusion tensor MRI as markers of neurodegeneration in amyotrophic lateral sclerosis. Brain Res 2010; 1348:156-64.

Mitusmoto H, Chad D, Pioro EP. Amyotrophic lateral sclerosis. Philadelphia: Oxford University Press, 1998.

Olney RK. The effects of executive and behavioral dysfunction on the course of ALS. Neurology 2005; 65:1774-1777.

Phukan J. Cognitive impairment in amyotrophic lateral sclerosis. Lancet Neurol 2007; 11:994-1003.

Plaitakis A. Abnormal glutamate metabolism in amyotrophic lateral sclerosis. Ann Neurol 1987; 22:575-579.

Rowland LP. Amyotrophic lateral sclerosis. N Engl J Med 2001; 22:1688-1700.

Yagishita A. Location of corticospinal tract in the internal capsule at MR imaging. Radiology 1994; 191:455-460.

Zhang LD. A three-dimensional fractal analysis method for quantifying white matter structure in human brain. Journal of Neuroscience Methods 2006; 150:242-253.

Zhang LD. Quantifying degeneration of white matter in normal aging using fractal dimension. Neurobiology of Aging 2007; 28:1543-1555.

CHAPTER II

MATERIALS AND METHODS

2.1. Subjects

A total of 100 subjects participated in the study and they were assigned into (1) a neurological control group (N=11, 51.7 ± 16.6 yrs, 3 females) and four patient groups according to their clinical signs and conventional MRI results: (2) 20 ALS patients with co-existing frontotemporal dementia (ALS-FTD group, 66.7 ± 9.9 yrs, 13 females), (3) 20 UMN-predominant ALS patients with CST hyperintensities (UMN-CST^{+} group; 52.9 ± 11.5 yrs, 7 females), (4) 27 UMN-predominant ALS patients without CST hyperintensities (UMN-CST^{-} group; 59.7 ± 11.9 yrs, 12 females), and (5) 22 classic ALS patients with an equal amount of UMN and LMN signs (ALS-classic group; 57.4 ± 11.5 yrs, 10 females). We were not the first to classify ALS patients based on their clinical signs. Cheung et al. divided ALS patients into three ALS subgroups based upon the UMN and LMN signs: (i) classic ALS, in which both UMNs and LMNs were affected; (ii) upper motor neuron type or primary lateral sclerosis, in which only central motor neurons (UMNs) were affected; and (iii) lower motor type or primary muscular atrophy, in which only LMNs were affected (Cheung et al., 1995). Some of the control subjects had

neurological disorders, such as Parkinson's disease and long-term headache. All the T1-weighted MRI data were obtained by a 1.5T scanner as routine clinical imaging data for patient evaluation. The Institutional Review Board at the Cleveland Clinic approved storage and de-identification of the images as part of the "Neuroimaging Registry/Database for CNS Analysis in Patients with Motor Neuron Disease".

2.2. Collection of MR Head Images

The 3D coronal MRI brain images of the whole cerebrum were obtained using a 1.5T Siemens Symphony (Erlangen, Germany) scanner by a process known as the magnetization prepared rapid gradient echo (MPRAGE) sequence. The following MPRAGE parameters were used for the image acquisition.

Parameter	Value
Slice Thickness	1 [mm]
Number of Slices	160
TR	1800 [ms]
TE	4.38 [ms]
TI	1100 [ms]
Flip Angle	10 [deg]
In-plate Resolution	1×1 [mm^2]

2.3. Image Processing

Figure 5 shows the steps involved in processing the coronal MRI brain images.

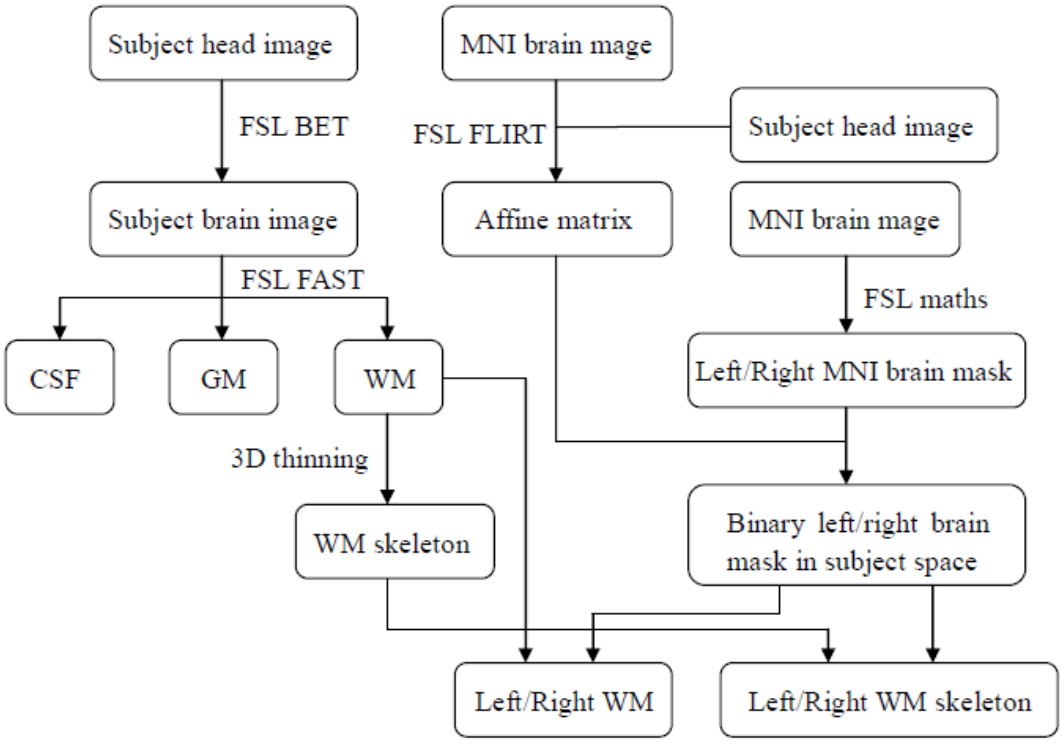

Figure 5: Image processing flowchart

2.3.1. Brain Extraction

The brain extraction step was processed using the Brain Extraction Tool (BET) in the FMRIB Software Library (FSL) package (Analysis Group, Center for Functional Magnetic Resonance Imaging of the Brain (FMRIB), Oxford, UK). The BET extracts the brain from the whole head image by removing non-brain tissue. There are currently three main methods to segment the brain tissue from the non-brain tissue: manual segmentation method, thresholding-with-morphology method, and surface model-based method. The BET basically uses deformable surface models which consist of a tessellated mesh of triangles. First, the centre-of gravity of the head image was found according to the intensity histogram. Then, a triangular tessellation of a sphere's surface was located

inside the head based on the pre-defined centre of gravity. Finally, the tessellation slowly deformed to the edge of the brain tissue by iteratively updating each vertex to surface until the final tessellated surface was self-intersecting. The surface of extracted brain was kept well spaced and smooth. Otherwise, the whole process would be repeated with a higher smoothness constraint (Smith, 2002).

2.3.2. Brain Tissue Segmentation (WM/GM/CSF)

The brain tissue segmentation step was carried out using FMRIB's Automated Segmentation Tool (FAST) in the FSL package. The extracted brain images from the BET were processed to produce three separate images: WM, GM, and corticospinal fluid (CSF). FAST is a statistical segmentation approach that generates an image with voxels of varying intensity that represent the proportion of each specific tissue present. During FAST, the bias field (intensity inhomogeneities in the RF field) was estimated and removed from the extracted brain images to prevent the intensity variations. To correct any spatial intensity variation, an algorithm presented by Guillemaud and Brady is used to facilitate segmentation. Lastly, the hidden Markov random field (HMRF) model was applied to encode the spatial information through the mutual influences of neighboring sites (Zhang et al., 2001).

2.3.3. Obtaining Skeleton

A 3D thinning method was applied to the binary images in order to obtain the skeleton (Ma and Sonka, 1996). A set of deleting templates (which are position configuration of object voxels and background voxels in a $3 \times 3 \times 3$ window) were designed to determine whether the boundary voxels should be removed. This approach eliminated

every parallel object voxel, satisfying at least one deleting template until no voxel could be deleted.

2.3.4. Separation of Left and Right Hemisphere

The hemispheres separation step was performed with the FSL FLIRT (FMRIB's Linear Image Registration Tool), which is an accurate and robust affine registration tool. The Montreal Neurological Institute (MNI) structural atlas (Jack Lancaster, Research Imaging Center, UTHSCSA, Texas) was also involved in the separation.

First, an affine matrix was calculated by registering the MNI 152 template to each brain image. Then, the left and right halves of the MNI brain were separated and transformed into subject space by applying the affine matrix to create hemisphere brain masks. Next, each hemisphere mask was multiplied with tissue images or skeleton images to produce a hemisphere of specific tissue or skeleton tissue (e.g. multiplying the left hemisphere mask with WM produced the left hemisphere of WM). Finally the hemisphere tissue images were saved as binary (black-and-white) images.

Figure 6 demonstrates the image processing results based on one sample slice from a control subject (Figure 6A, C, E) and one sample slice from an ALS-FTD subject (Figure 6B, D, F). The WM segmentation results indicated that the FAST method segmented WM of the brain well (see Fig legend for details).

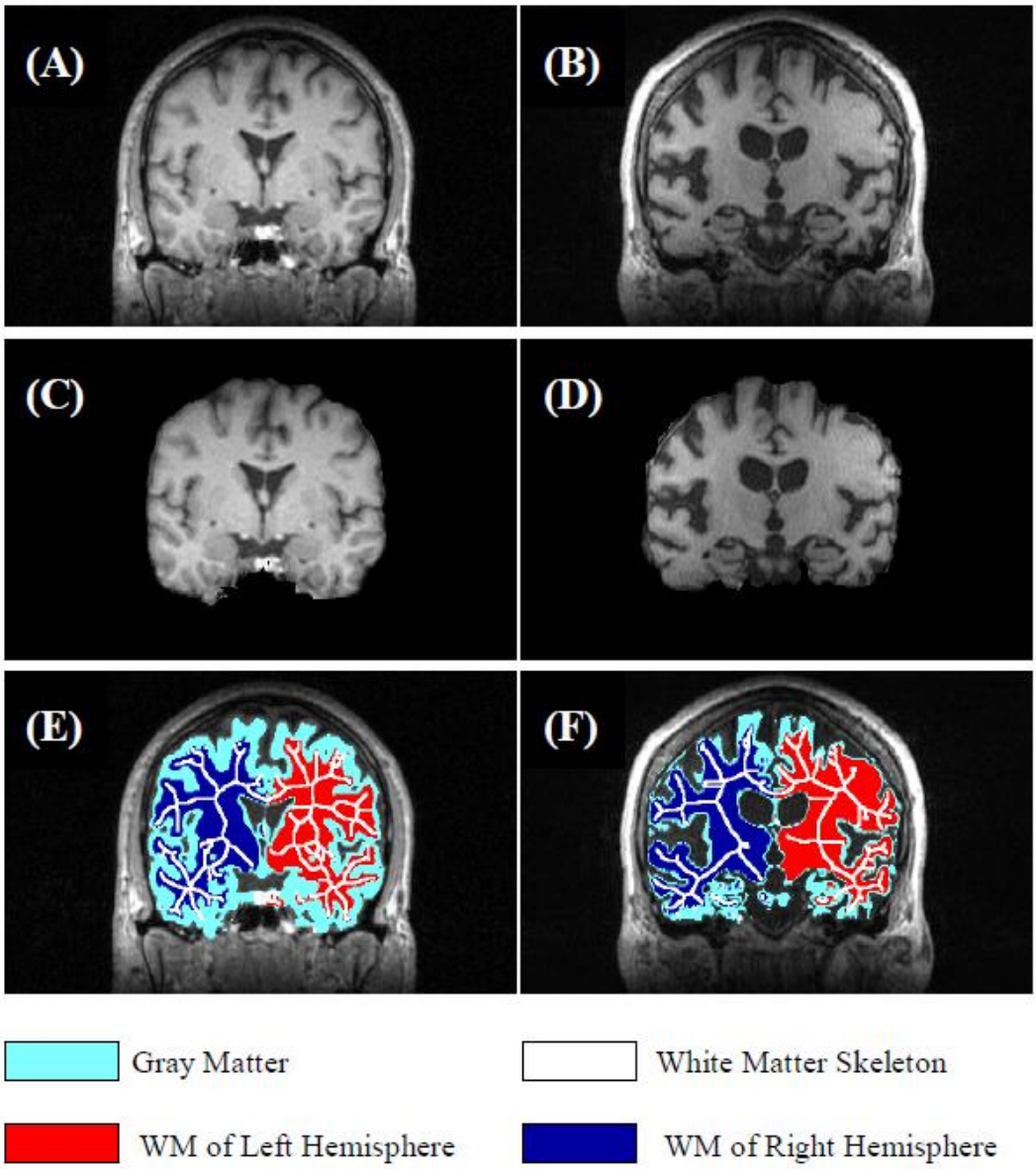

Figure 6: Image processing results based on one sample slice from one control subject (A,C,E) and one sample slice from one ALS-FTD subject (B,D,F). Images on left column are the processing results for the control subject: (A) T1-weighted head image; (C) Brain extraction result; (E) Brain tissues and WM skeleton overlaid onto the original head image. Images on right column are the processing results for the ALS-FTD subject: (B) T1-weighted head image; (D) Brain extraction result; (F) Brain tissues and WM skeleton overlaid onto the original head image.

2.4. Fractal Analysis

In general, FD serves as an index of morphometric variability and complexity of an object. A higher FD value refers to a more complicated structure. There are three forms of

FDs in this study: skeleton FD, surface FD, and the general structure FD. The skeleton FD and the surface FD serve as the index to detect the interior structure and surface degeneration respectively. The general structure FD is the index to assess the WM atrophy. Because the skeleton physiologically represents the complexity of the WM fiber bundle connectivity network (e.g. fiber crossing, bifurcation), a declined skeleton FD means the degeneration of WM fibers. The surface is the interface between the GM and WM, representing the facial convolution, therefore a lower surface FD means a smoother facial structure. A reduced general structure FD tells that WM volume decreased.

The 3D box-counting method derived from the Harmonic and Fractal Image Analyzer (HarFA) was applied to calculation of the fractal dimension of defined structure (Zhang et al., 2006). The entire process consists of three major steps: (i) counting the number of boxes covering the skeleton or WM structure; (ii) performing linear regression analysis to obtain the slope value, which was the initial FD; and (iii) performing single slope analysis to get the accurate FD. In the third step, different thresholds were applied to improve accuracy of FD calculation.

Using the HarFA counting mechanism, the image was divided into three different parts after applying the box-mesh: the background, the object and the boundary of the object. The HarFA counted three categories of boxes belonging to those three separate areas: (i) N_B, which covered only the black background; (ii) N_W, which contained only the object area; and (iii) N_{BW}, which covered the border of object and contained part of the white object and part of the black background (Figure 7). As a result, there were three different FDs (FD_B, FD_W, FD_{BW} correlated with N_B, N_W and N_{BW} respectively) representing the properties of the black background, the white object, and the boundary

of the object. The traditional box-counting dimension was FD_{WBW} which was determined by the sum of N_W and N_{BW} (N_{WBW}).

(A) 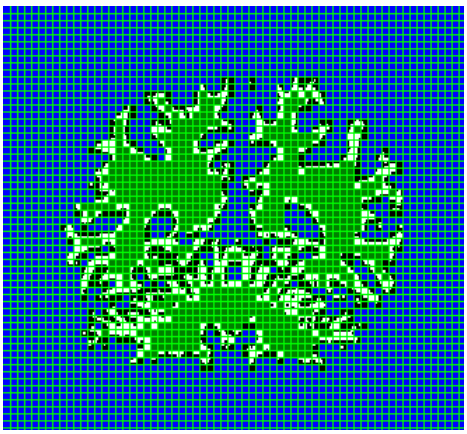 (B) 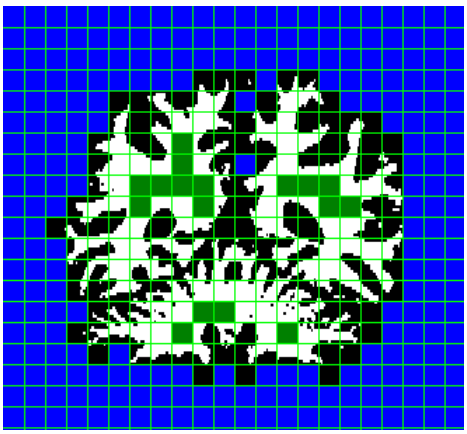

Figure 7: 2D box-counting method in HarFA. Mesh with different-sized boxes (r) was put to cover the 2D sample binary WM slice. Number of boxes (N_W) which cover the object WM (green boxes), number of boxes (N_B) which cover the black background (blue boxes) and number of boxes (N_{BW}) which cover the boundary between WM and black background (rest boxes). The images were generated by the box-counting package from HarFA (http://www.fch.vutbr.cz/lectures/imagesci/) using data from one subject.
(A) r=5 pixels, N_W=557, N_B=2688.3157, N_{BW}=729; (B) r=15 pixels, N_W=17, N_B=244.5911, N_{BW}=180.

2.5. Statistical Analysis

A one-way analysis of variance (ANOVA) (control vs. ALS-FTD vs. UMN-CST$^+$ vs. UMN-CST$^-$ vs. ALS-classic groups) was conducted to analyze the WM structure of the whole brain to determine the disease effects on the WM FDs. A two-way repeated measures ANOVA (within factor, left vs. right hemispheres; between factor, control vs. ALS-FTD vs. UMN-CST$^+$ vs. UMN-CST$^-$ vs. ALS-classic groups) was performed separately to detect the left-right hemispheric asymmetry of the WM structure in each group and compare that information among the groups. Significant differences were accepted at $P \leq 0.05$. Generalized linear model was used to fit the one-way or two-way ANOVA in this study. The type III F-statistics and p-values were calculated based on the F statistics. Spearman's rank correlation coefficient analysis was carried out to determine

the relationship between scores of ALS function evaluation and FD of brain WM structures.

2.6. Reference

Cheung G. Amyotrophic lateral sclerosis: correlation of clinical and MR imaging findings. Radiology 1995; 194:263-270.

Ma CM, Sonka M. A fully parallel 3D thinning algorithm and its applications. Computer Vision and Imaging Understanding 1996; 64:420-33.

Smith SM. Fast robust automated brain extraction. Human brain mapping 2002; 17: 143-155.

Zhang LD. A three-dimensional fractal analysis method for quantifying white matter structure in human brain. Journal of Neuroscience Methods 2006; 150:242-253.

Zhang Y. Segmentation of brain MR images through a hidden Markov random field model and the expectation-maximization algorithm. IEEE Trans Med Imaging 2001; 20:45-57.

CHAPTER III

RESULTS

Fractal dimension (FD) of white matter (WM) of each hemisphere as well as the entire brain was evaluated on three separate structural forms: skeleton, surface, and general structure. The WM skeleton represents the interior structure patterns and reveals paths of WM tracts that contain axons of neurons connecting different neural populations. The WM surface is the facial convolution pattern of the system. The WM general structure refers to the entire shape patterns. The results of three forms of WM FDs were shown in the Table I.

3.1. Disease Effect on WM Structure Changes

Comparisons of FD values of the three WM structural forms were made in each hemisphere and the whole brain among the ALS subgroups. FD differences in WM skeleton, surface, and general structure of the left or right hemisphere by post hoc tests and those of whole WM by one-way analysis of variance (ANOVA) among the ALS subgroups are shown in Figures 8-10 and Tables II-IV. In all figures, each bar graph is the

FD mean in a given group and the corresponding error bar refers to standard deviation of the mean.

3.1.1. WM Interior (Skeleton) Structure Complex

With respect to skeleton, the UMN-CST^{+} group has the most complex interior pattern while the ALS-FTD group has the simplest interior structure. The FD of the WM skeleton in the left hemisphere was significantly greater in the UMN-CST^{+} group when compared with the ALS-FTD group (P=0.033) and the UMN-CST^{-} group (P=0.043) (Figure 8A). The WM skeleton FD in the right hemisphere was markedly greater in the UMN-CST^{+} group than the other ALS groups with P<0.001 (compared with ALS-FTD), P=0.005 (with UMN-CST^{-}), and P=0.024 (with ALS-classic) (Figure 9A). When the whole brain WM skeletons were compared among the groups, significant differences were observed between the control and ALS-FTD (P=0.028), ALS-FTD and UMN-CST^{+} (P<0.001), ALS-FTD and ALS-classic (P=0.024), UMN-CST^{+} and UMN-CST^{-} (P=0.001), and UMN-CST^{+} and ALS-classic (P=0.013) (Figure 10A). The WM skeleton FD data show different complexity patterns among the studied groups.

3.1.2. WM Surface (Convolution Pattern) Complexity

FD in the WM surface had no significant differences among the five groups in both left and right hemispheres (Figure 8B and 9B). The WM surface FD for the whole brain was greater only in the ALS-classic group when compared to the UMN-CST^{-} group (P=0.049) (Figure 10B). These results suggest that the complexity of WM surface structure was almost the same among all five groups with exception of more complicated surface structure between the ALS-classic and the UMN-CST^{-} groups.

3.1.3. WM General Structure Complexity

The UMN-CST^{+} group exhibited significantly greater WM general structure complexity than the UMN-CST^{-} group when both the right hemisphere (P=0.019) and the whole brain (P=0.004) were compared (Figure 9C and 10C). FD of the WM general structure for the whole brain was also greater in the UMN-CST^{+} than the ALS-classic (P=0.045) groups. FD of the WM general structure for the whole brain was significantly smaller in the ALS-FTD group than the control (P=0.008), UMN-CST^{+} (P<0.001) as well as the ALS-classic (P=0.021) groups. In general, the WM general structure complexity showed remarkable changes among the groups only in the whole brain with the least FD reduction in the UMN-CST^{+} group and the greatest reduction in the ALS-FTD group.

Table 3.1. Results of white matter fractal dimension

region	control	ALS-FTD	UMN-CST^{+}	UMN-CST^{-}	ALS-classic
Skeleton					
Left	2.407±0.018	2.404±0.030	2.420±0.022	2.406±0.027	2.412±0.022
Right	2.409±0.021	2.394±0.023	2.420±0.021	2.400±0.025	2.403±0.019
Whole	2.487±0.018	2.469±0.020	2.501±0.024	2.480±0.023	2.484±0.017
Surface					
Left	2.462±0.018	2.468±0.020	2.467±0.015	2.464±0.019	2.471±0.013
Right	2.467±0.024	2.465±0.017	2.472±0.013	2.465±0.022	2.468±0.014
Whole	2.549±0.017	2.551±0.020	2.557±0.013	2.547±0.019	2.557±0.014
General Structure					
Left	2.582±0.054	2.572±0.044	2.590±0.035	2.582±0.044	2.590±0.041
Right	2.598±0.020	2.583±0.016	2.603±0.033	2.575±0.048	2.581±0.050
Whole	2.633±0.013	2.618±0.013	2.638±0.015	2.625±0.015	2.629±0.015

Mean±Standard deviation. Left, left hemisphere WM. Right, right hemisphere WM. Whole, whole WM

Table I: Results of white matter fractal dimension

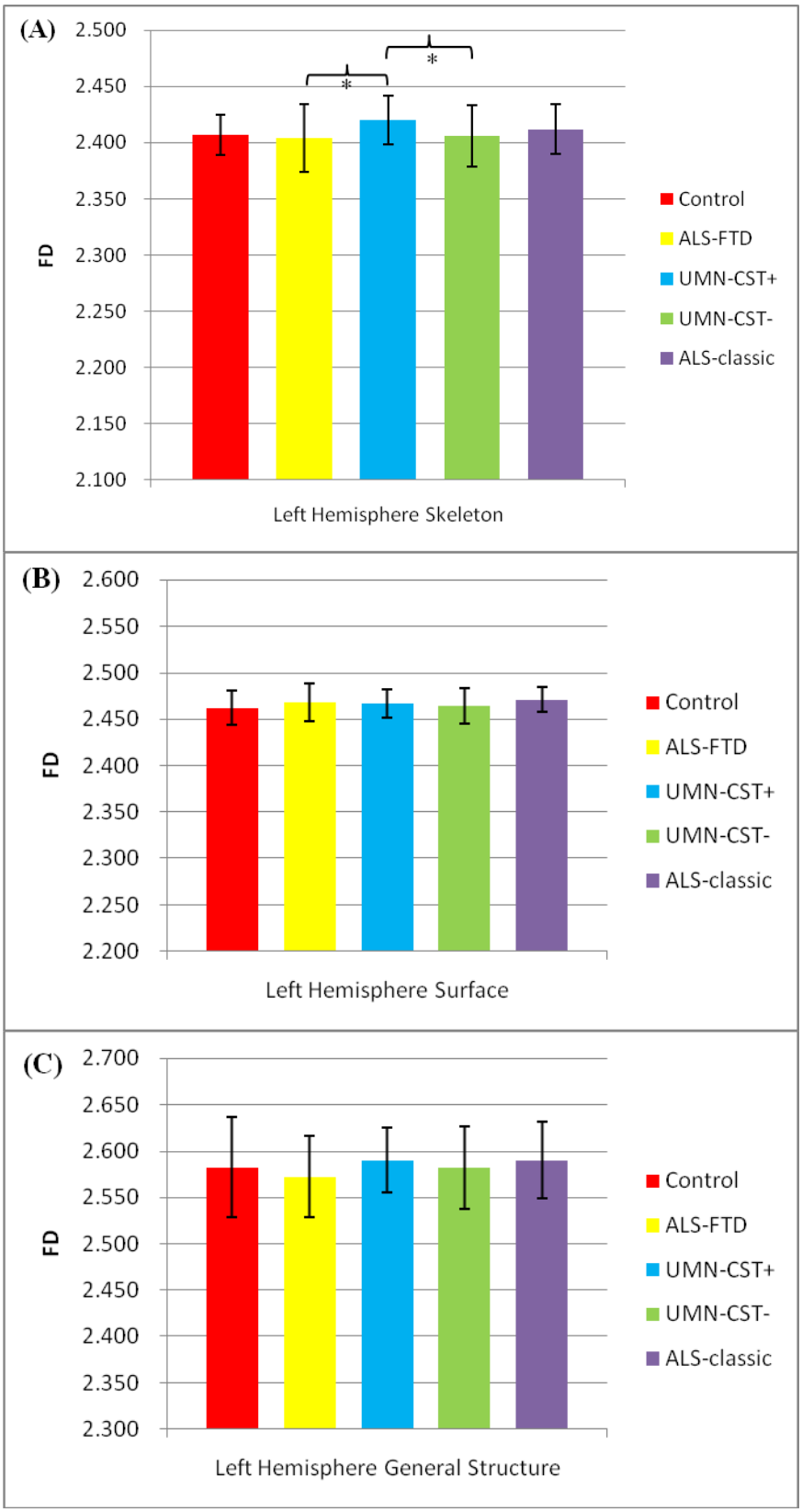

Figure 8: Left hemisphere WM FD results of five groups. (A) skeleton, (B) surface, and (C) general structure. *P<0.05, **P<0.01

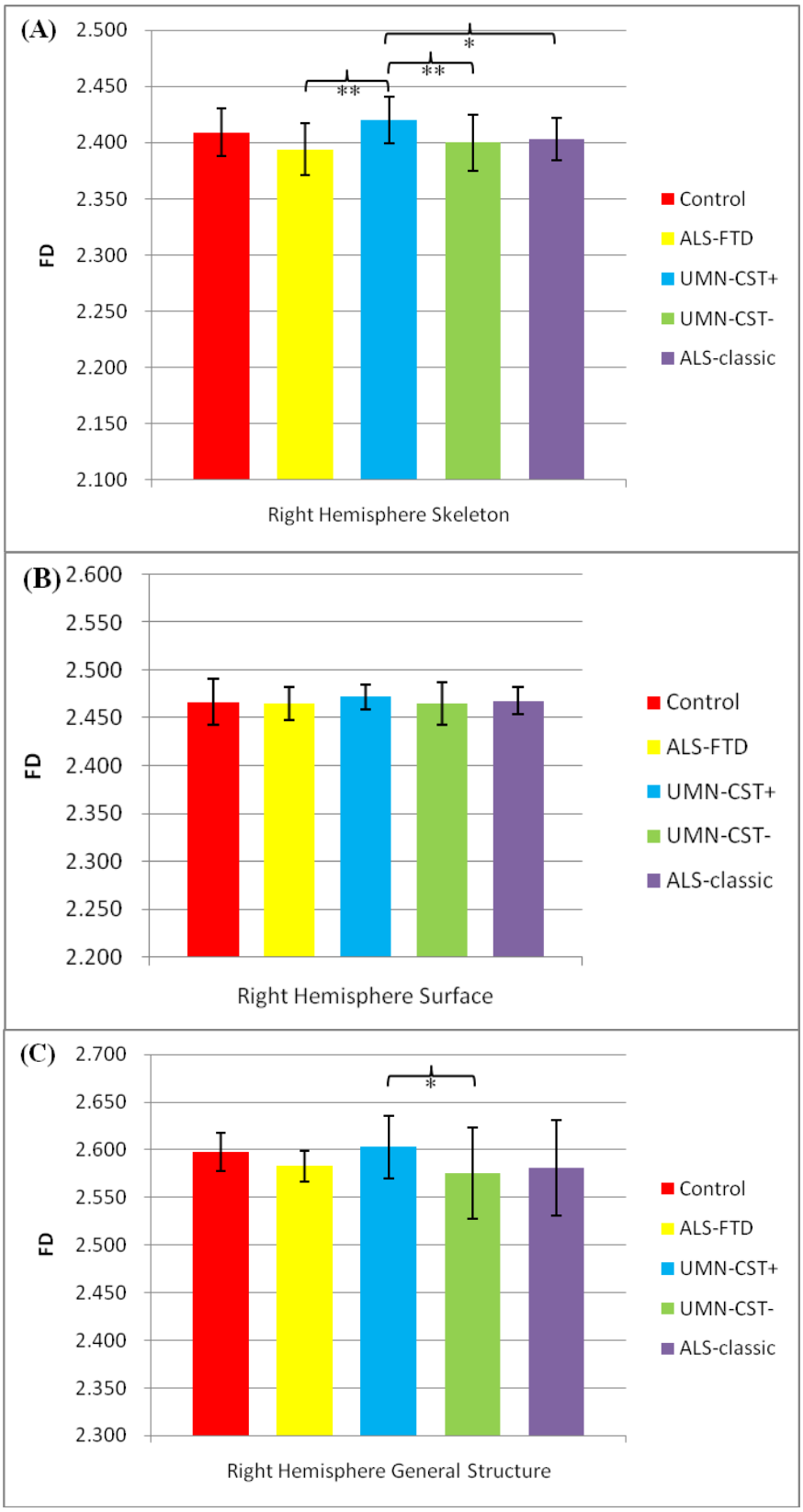

Figure 9: Right hemisphere WM FD results of five groups. (A) skeleton, (B) surface, and (C) general structure. *P<0.05, **P<0.01

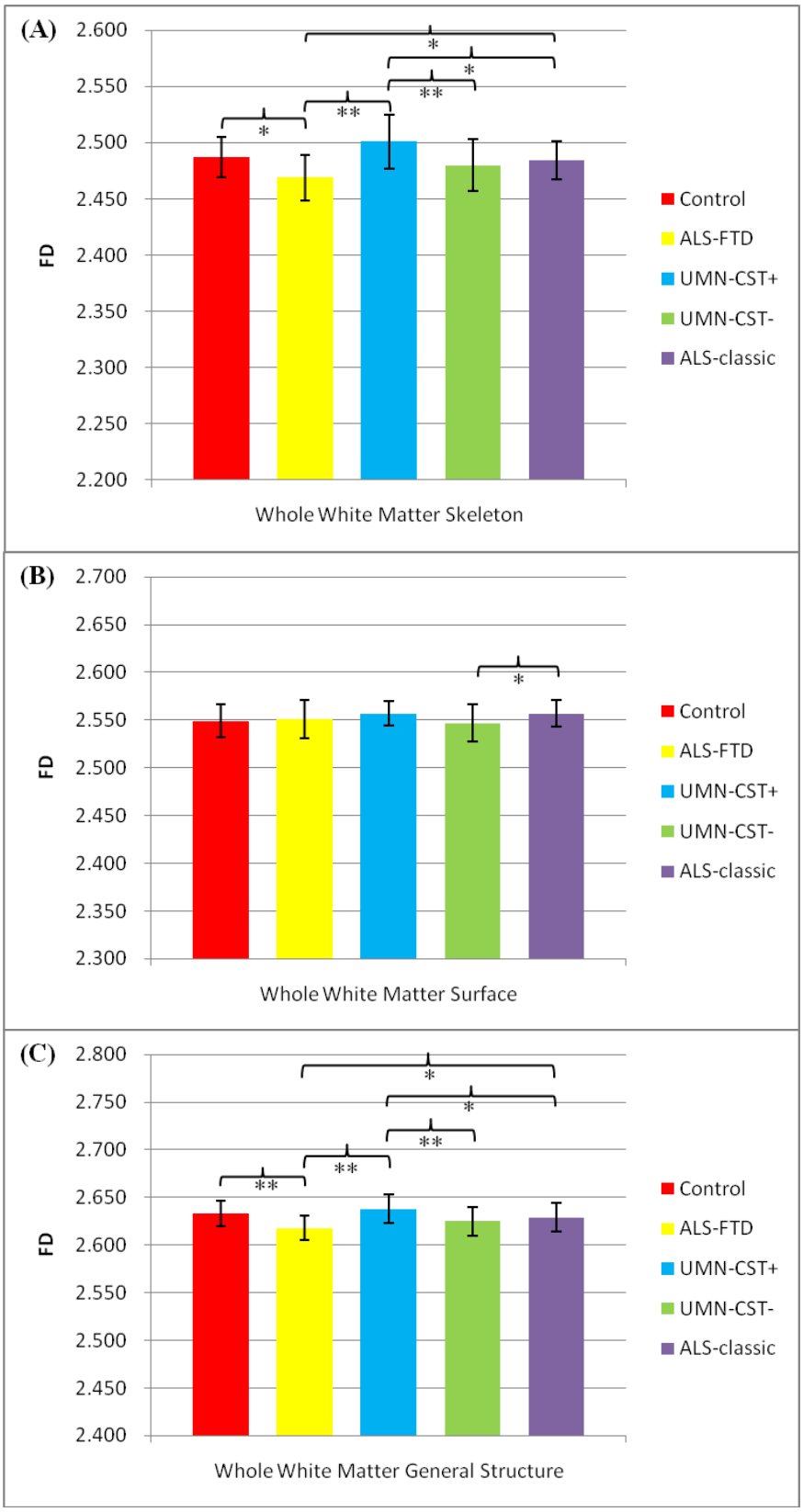

Figure 10: Whole brain WM FD results of the five groups. (A) skeleton, (B) surface, and (C) general structure. *P<0.05, **P<0.01

Table II: Two-way repeated measures ANOVA *P* value on white matter fractal dimension between groups in left hemisphere skeleton, surface, and general structure

Group	Skeleton		Surface		General Structure	
	LS means	SE	LS means	SE	LS means	SE
Control	2.407	0.007	2.462	0.005	2.582	0.012
ALS-FTD	2.404	0.005	2.468	0.004	2.572	0.009
UMN-CST^{+}	2.420	0.005	2.467	0.004	2.590	0.009
UMN-CST^{-}	2.406	0.005	2.464	0.003	2.582	0.008
ALS-classic	2.412	0.005	2.471	0.004	2.591	0.009
F value	1.36		0.83		0.64	
P value	0.254		0.509		0.633	

SE=standard error, LS means=least squares means (**P*<0.05, ***P*<0.01)

Table III: Two-way repeated measures ANOVA *P* value on white matter fractal dimension between groups in right hemisphere skeleton, surface, and general structure

Group	Skeleton		Surface		General Structure	
	LS means	SE	LS means	SE	LS means	SE
Control	2.409	0.007	2.467	0.005	2.598	0.012
ALS-FTD	2.394	0.005	2.465	0.004	2.583	0.009
UMN-CST^{+}	2.420	0.005	2.472	0.004	2.603	0.009
UMN-CST^{-}	2.400	0.005	2.465	0.003	2.575	0.008
ALS-classic	2.404	0.005	2.468	0.004	2.581	0.009
F value	4.00		0.47		1.99	
P value	0.005**		0.759		0.102	

SE=standard error, LS means=least squares means (**P*<0.05, ***P*<0.01)

Table IV: One-way ANOVA *P* value on white matter fractal dimension between groups in whole brain white matter skeleton, surface, and general structure

Group	Skeleton		Surface		General Structure	
	LS means	SE	LS means	SE	LS means	SE
Control	2.487	0.006	2.549	0.005	2.633	0.004
ALS-FTD	2.469	0.005	2.551	0.004	2.618	0.003
UMN-CST^{+}	2.501	0.005	2.557	0.004	2.638	0.003
UMN-CST^{-}	2.480	0.004	2.547	0.003	2.625	0.003
ALS-classic	2.484	0.004	2.557	0.004	2.629	0.003
F value	5.86		1.56		5.15	
P value	<0.001**		0.191		0.001**	

SE=standard error, LS means=least squares means (**P*<0.05, ***P*<0.01)

3.2. Asymmetry of WM Structure Complexity between Left and Right Hemispheres

The WM structural complexity between the two hemispheres was analyzed using repeated measures ANOVA. In general, the structural complexity was symmetrical in all groups except that the skeleton FD was significantly smaller ($P<0.05$) for right than left hemispheres in ALS-FTD and ALS-classic groups (Figure 11 A, B, and C). This indicates that only the interior WM structure (skeleton) was asymmetrical between the hemispheres in only ALS-FTD and ALS-classic groups. The actual FD values for between-hemisphere comparisons among the groups are shown in Table V (skeleton), Table VI (surface) and Table VII (general structure).

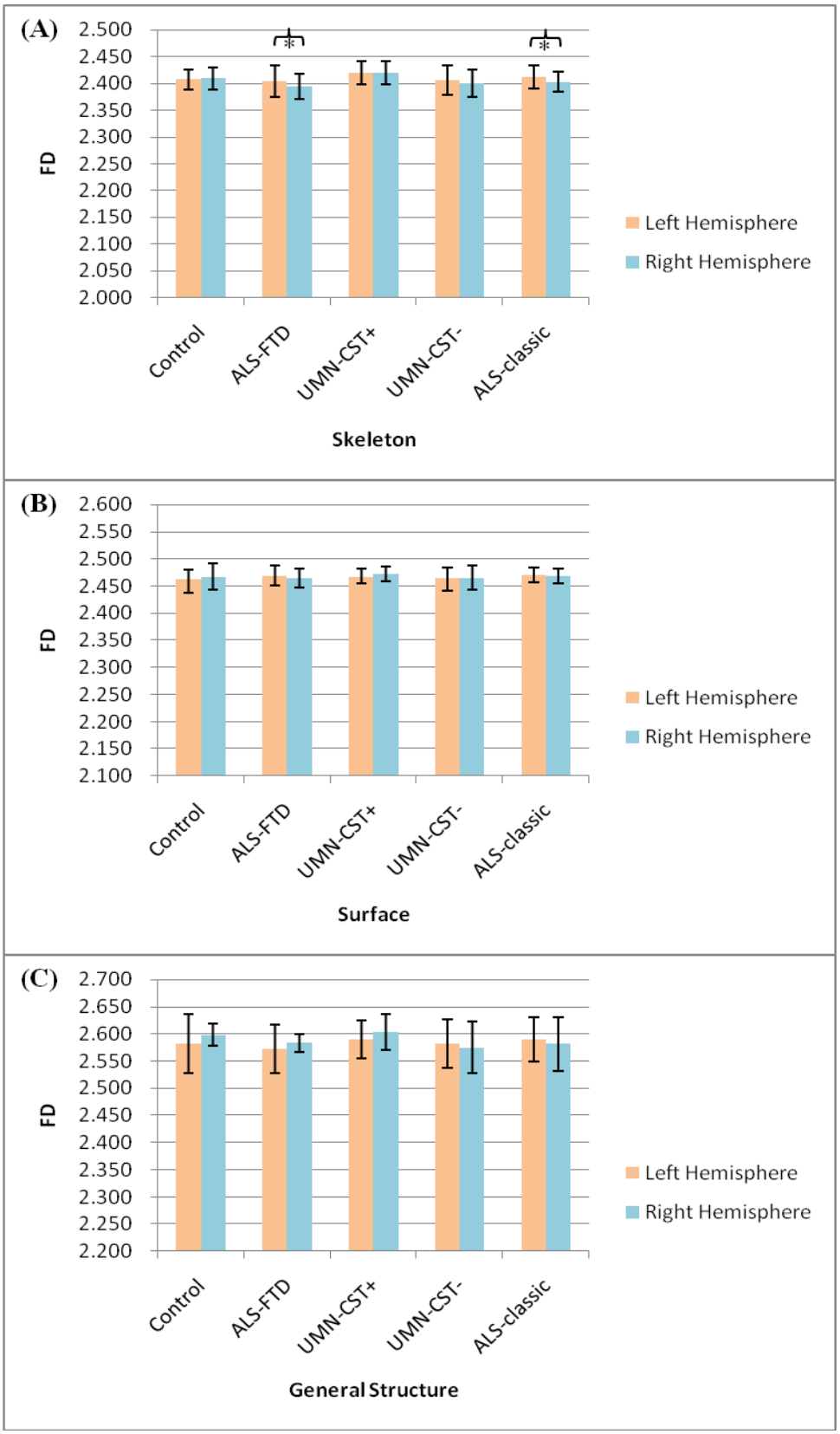

Figure 11: Histogram of WM FD results in left and right hemispheres for the (A) skeleton, (B) surface, and (C) general structure

Table V: Results of two-way repeated measures ANOVA for hemispheric WM skeleton FD comparisons

Group	Left Hemisphere		Right Hemisphere		t value	*P* value
	LS means	SE	LS means	SE		
Control	2.407	0.007	2.409	0.007	-0.21	0.837
ALS-FTD	2.404	0.005	2.394	0.005	2.27	0.025*
UMN-CST^{+}	2.420	0.005	2.420	0.005	0.02	0.982
UMN-CST^{-}	2.406	0.005	2.400	0.005	1.50	0.138
ALS-classic	2.412	0.005	2.404	0.005	2.05	0.043*

SE=standard error, LS means=least squares means (*P<0.05, **P<0.01)

Table VI: Results of two-way repeated measures ANOVA for hemispheric WM surface FD comparisons

Group	Left Hemisphere		Right Hemisphere		t value	*P* value
	LS means	SE	LS means	SE		
Control	2.462	0.005	2.467	0.005	-1.26	0.209
ALS-FTD	2.468	0.004	2.465	0.004	1.11	0.271
UMN-CST^{+}	2.467	0.004	2.472	0.004	-1.60	0.112
UMN-CST^{-}	2.464	0.003	2.465	0.003	-0.54	0.594
ALS-classic	2.471	0.004	2.468	0.004	1.25	0.214

SE=standard error, LS means=least squares means (*P<0.05, **P<0.01)

Table VII: Results of two-way repeated measures ANOVA for hemispheric WM general structure FD comparisons

Group	Left Hemisphere		Right Hemisphere		t value	*P* value
	LS means	SE	LS means	SE		
Control	2.582	0.012	2.598	0.012	-1.28	0.202
ALS-FTD	2.572	0.009	2.583	0.009	-1.24	0.216
UMN-CST^{+}	2.590	0.009	2.603	0.009	-1.44	0.154
UMN-CST^{-}	2.582	0.008	2.575	0.008	0.89	0.374
ALS-classic	2.591	0.009	2.581	0.009	1.11	0.271

SE=Standard Error, LS means=Least Squares Means (*P<0.05, **P<0.01)

CHAPTER IV

DISCUSSION

The main findings of this were that (i) ALS patients with dementia (ALS-FTD) had greatest brain WM degeneration (showing by FD-measured WM structural complexity) among the four ALS groups, as well as compared with the control group. (ii) ALS patients without hyperintensity signals in the CST (UMN-CST^{-}) exhibited second worst WM structural degeneration among the analyzed groups, followed by patients with classic ALS signs (ALS-classic). (iii) Brain WM structure was least affected in ALS patients with hyperintensity signals in the CST (UMN-CST^{+}) among the four ALS groups, which was comparable with and many times even slightly better than the WM structure of the control group. (iv) Among the three forms of brain WM structure measured, skeleton seemed to be the most sensitive form fro detecting WM structural degeneration followed by general structure and surface. (v) FD structural analysis in the whole brain was more sensitive than in a single hemisphere in detecting brain WM structural degeneration. (vi) Brain WM structure complexity indicated by skeleton FD was asymmetrical in the ALS-FTD and ALS-classic groups with a higher complexity measure for the left hemisphere. These results are discussed below.

4.1. WM of ALS-FTD Patients

The ALS-FTD group showed significant decreases in FD of the left and right hemisphere skeleton compared with UMN-CST^{+} group and in FD of the whole brain skeleton compared with control, UMN-CST^{+}, and ALS-classic groups. For the general structure, ALS-FTD patients had significantly reduced FD of the whole brain relative to the control, UMN-CST^{+}, and ALS-classic groups. No difference in FD of surface structure between ALS-FTD and any of other groups (Figures 8-10).

Although patients in ALS-FTD group have symptoms of both ALS and FTD, it is believed that FTD is the main cause of the observed decline of skeleton and general structure FD measures. Since the FD measurements of WM is determined by the complexity level of the brain WM fiber bundle connectivity network (such as fiber crossings and bifurcations), the decreased FD of the WM structure, especially skeleton structure, indicates a weakened connectivity in the WM network. A significant reduction in brain WM structural complexity level in ALS-FTD patients may be a consequence of WM loss (Boxer et al., 2010) as a result of GM loss throughout the frontal and temporal lobes in ALS-FTD patients (Rajagopalan, 2010). GM loss along with abnormal diffusivity in WM tracts connecting the affected GM regions contributed to the damage of neuronal network in white matter, particularly in the fontal and temporal lobes (Whitwell et al., 2010).

Although some of the control subjects suffered other neurological diseases such as Parkinson's disease and chronic headache, this group on average, did not have GM or WM atrophy in the frontal and temporal lobes and the WM fiber bundle connectivity network was not afflicted remarkably. This was also true for the UMN-CST^{+} group

(Rajagopalan, 2010). In that case, the skeleton FD and general structure FD of control and UMN-CST^{+} groups were higher than those of the ALS-FTD group.

Figure 12 shows 2D images of WM skeletons of a control (left), ALS-FTD (middle), and UMN-CST^{+} (right) subject in each row of images (upper row: horizontal plane, lower row: coronal plane). The extracted 2D skeletons, colored in yellow, are overlaid onto the corresponding T1-weighted head images. These skeleton images show inner structure of the WM system. It is clear from the 2D WM images on both horizontal and coronal planes that the skeletons of the ALS-FTD patient are distributed loosely and have fewer branches compared those of the control subject and UMN-CST^{+} patient. This would indicate a lower level of WM structural complexity level in ALS-FTD than other two subjects.

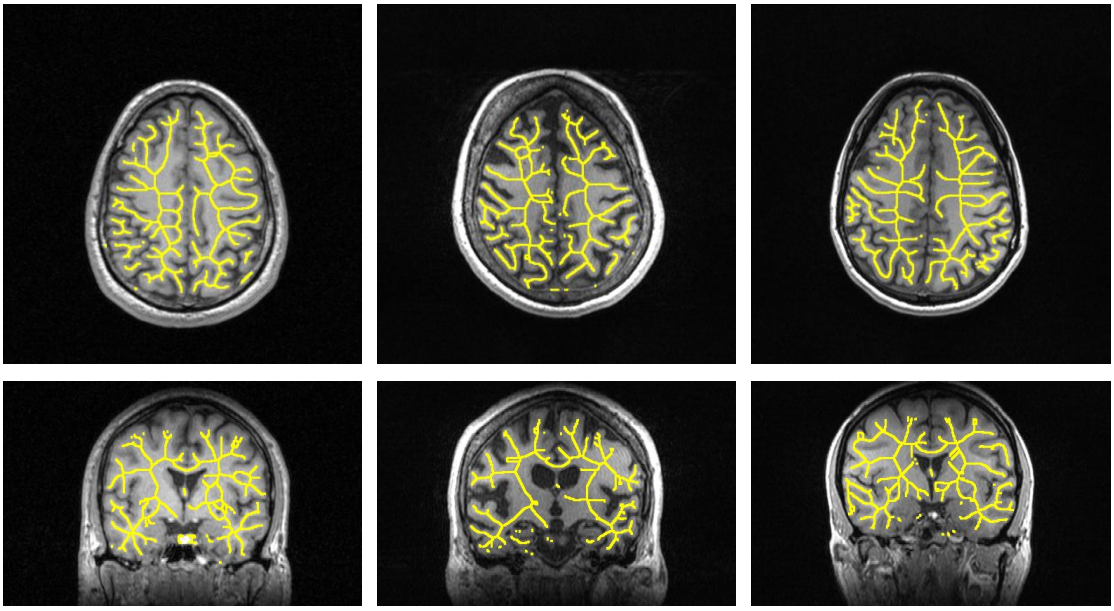

Figure 12: Illustration of 2D WM skeletons in two planes: horizontal plane (upper row) and coronal plane (lower row). In each row, an image of a control (left), ALS-FTD (middle), and UMN-CST^{+} (right) subject is displayed. The ALS-FTD patient shows the lowest complexity level in the WM skeleton structure among the three subjects.

Images in Figure 13 show WM structural differences among the three subjects by qualitative comparisons of non-GM and non-WM areas. In each image, light blue areas represent GM and dark blue (right hemisphere) and red (left hemisphere) areas show WM tissues. It is clear that the ALS-FTD patient (middle image in each row) is with noticeably larger non-brain tissue areas than either the control (left image) or UMN-CST^{+} (right image) subject, especially the gap between the two hemispheres. The increased non-brain tissue areas in ALS-FTD may be related to a decline in WM structure complexity level in this group of patients.

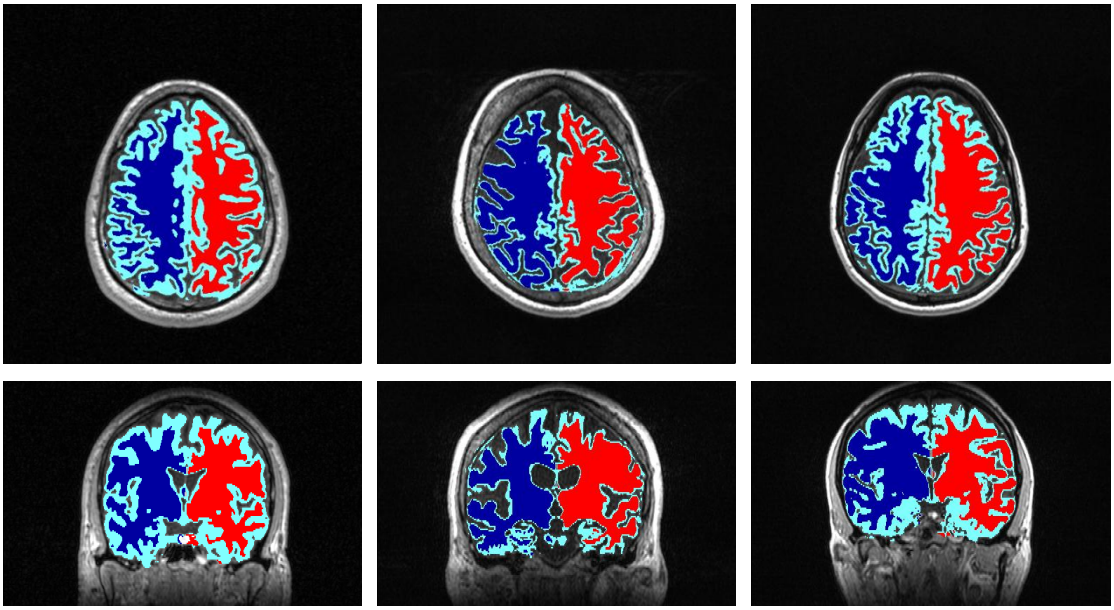

Figure 13: Illustration of the left (red) and right (blue) hemisphere WM in horizontal (upper row) and coronal (lower row) planes of a control (left image in each row), ALS-FTD (middle image), and UMN-CST^{+} (right image) subject. Light blue color areas represent GM. The ALS-FTD patient exhibits larger non-brain tissue areas.

4.2. WM of UMN-CST^{+} Patients

ALS patients in UMN-CST^{+} group showed higher FD measures in WM skeleton structure than all other three ALS subgroups in each hemisphere (except ALS-classic group in left hemisphere) as well as the whole brain. For the WM general structure, the

UMN-CST^{+} group had higher FD values in the whole brain than all other three ALS subgroups, and than UMN-CST^{-} group in the right hemisphere. These findings suggest that complexity of the interior and general WM structures of UMN-CST^{+} patients was less affected than the other ALS groups.

Although it has been suggested that the mechanism of hyperintensity along the CST is either the result of Wallerian degeneration (Prodan and Holland, 2002) or due to a dying back process (Lee et al., 2003), the exact cause of the hyperintensity is still unknown. Even less is known of why ALS patients with CST hyperintensity do not experience as much changes in brain WM structural complexity than other ALS patient groups. It could be related to differences in the degree of nerve degeneration or the rate of nerve regeneration among various types of ALS disease.

Because ALS is a progressively degenerative disorder, the degeneration gets worse with duration of ALS symptoms. Figure 14 shows that ALS patients in UMN-CST^{+} group have a significantly shorter duration of symptoms than the UMN-CST^{-} and ALS-classic groups ($P < 0.001$ and 0.016, respectively). Consistent with the results of this, the degree of degeneration in the WM structure complexity of these two groups was more severe than the UMN-CST^{+} group. As a result, by comparing two groups of ALS patients with predominant UMN signs with and without CST hyperintensity, less affected WM structure in UMN-CST^{+} patients could probably be related to their short duration of the symptoms. Also, a significantly shorter duration of symptoms in ALS-classic group than that in UMN-CST^{-} group ($P < 0.05$) was found, which could explain the reason of why the ALS-classic group has a more complicated surface than UMN-CST^{-} group.

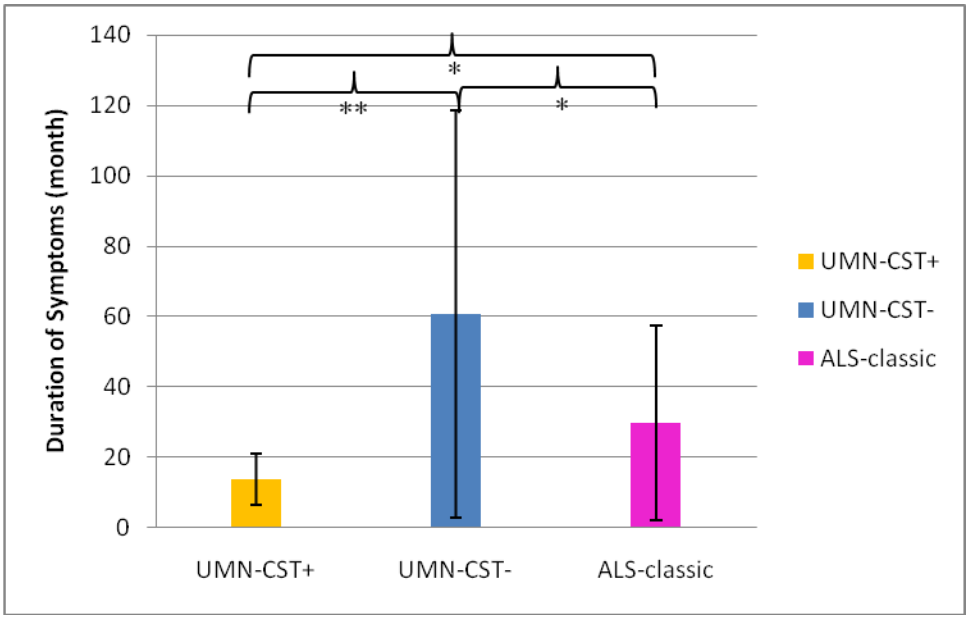

Figure 14: Comparison of symptom duration among UMN-CST^{+}, UMN-CST^{-} and ALS-classic groups. Patients in UMN-CST^{+} group had shortest symptom duration.

Regeneration occurs in both the central nervous system (CNS) and peripheral nervous system (PNS), even in ALS and can rectify or slow down, to a certain degree the degeneration process (Hilliard, 2009). Neuroregeneration in the PNS occurs to a significant degree (Yiu and He, 2006), while injury to the CNS is not followed by extensive regeneration. In PNS, axonal sprouts from at the proximal segment grow until they enter the distal segment, and the growth is governed by chemotactic factors secreted from Schwann cells or neurolemmocyte. In CNS, regeneration is limited by the inhibitory influences of the glial and extracellular environment. For example glial scars actually produce factors that inhibit remyelination and axon repair (Yiu and He, 2006; Karnezis et al., 2004; Bregman et al., 1995). After the recovery of the axon, the fiber could reinnervate the original target muscle to restore original functionality. To summarize, both UMN and LMN regeneration rates are controlled by some other factors (e.g. chemotactic factors, glial scars).

In ALS, Nogo-A is a key factor in restricting regeneration and repair of injured

axons, which increases the regulation level by a reduced expression of Nogo-A (GrandPre et al., 2002; Jokic et al., 2006; Karnezis et al., 2004). The regeneration rates and degree of nervous system recoveries of different ALS subgroups may diverge due to differences in the control factors (e.g. expression level of Nogo-A). Furthermore, more fatty tissue (e.g. myelin) is indicated by hyperintensity in T2-weighted images, meaning the hyperintensity along CST probably represents fiber remyelination and axon regeneration. If so, it is logic to see the UMN-CST^{+} group to have a relatively more complex WM connectivity network compared with the other ALS patient subgroups. The results of the research presented here agree with this assumption.

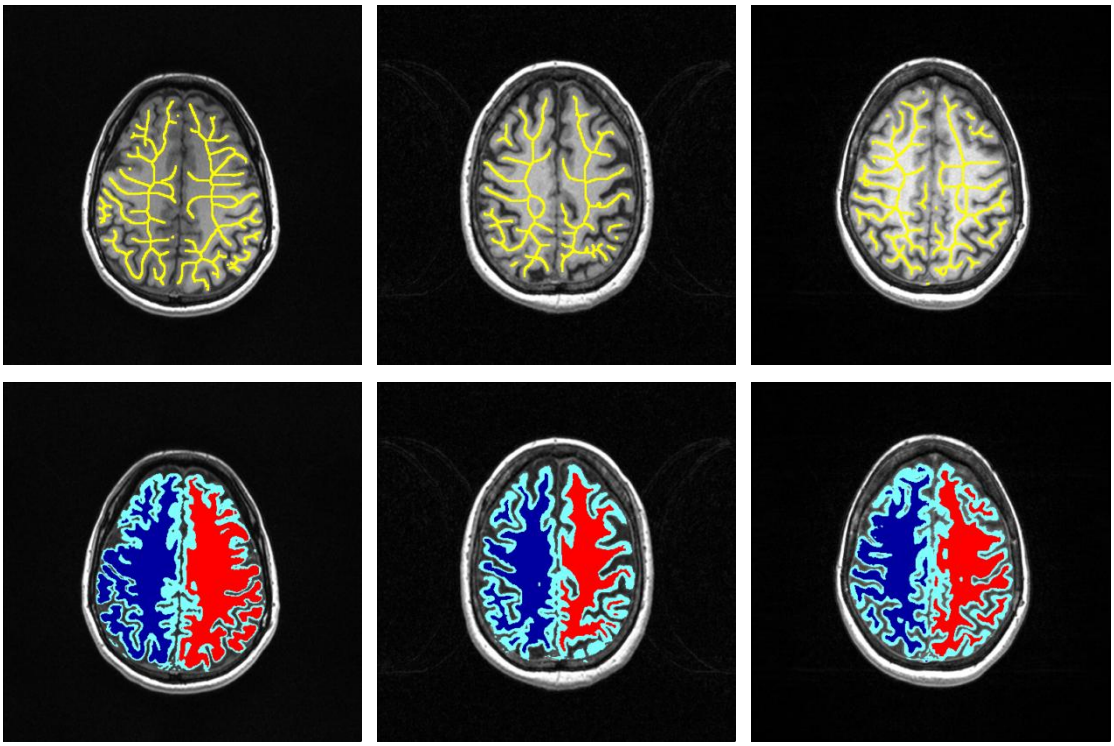

Figure 15: Illustration of 2D WM skeletons (upper row) and left (red) and right (blue) hemispheres of WM in horizontal plane in a UMN-CST^{+} (left image in each row), UMN-CST^{-} (middle image),and ALS-classic (right image) subject. The skeleton structure shows a more complex pattern in UMN-CST^{+} than UMN-CST^{-} and ALS-classic groups.

In 2D skeleton images (Figure 15), one can deduce that WM skeletons of the UMN-CST^{+} subject (upper row, left image) is more tightly packed than the UMN-CST^{-} (middle image) and ALS-classic (right image) groups. As a result, the WM interior structure shows a more complex pattern than the other two groups.

Images in lower row in Figure 15 indicate that the volume of WM (blue and red colors) is larger in UMN-CST^{+} patient (left Image) than UMN-CST^{-} (middle image) and ALS-classic (right image) patient.

4.3. Correlation between ALSFRS-R Scores and FDs

Amyotrophic lateral sclerosis functional rating scale revised (ALSFRS-R) is a standardized score indicating functional status of ALS patients. It scales the total functional disability with a range from 0 (maximum disability) to 48 (normal) points. It is a widely-used tool for evaluation of functional status and disease progression in ALS patients.

By calculating the Spearman's rank correlation coefficient (r_s) for the skeleton FD, surface FD, and general structure FD with the ALSFRS-R scores, it was found that the FDs increase with the ALSFRS-R score. A correlation coefficient of 0.42 (P = 0.0001, Figure 16A) was found between the skeleton FD, 0.40 between the surface FD and ALSFRS-R (P = 0.0002), Figure 16B), and 0.38 between general structure FD and ALSFRS-R (P = 0.0004, Figure 16C).

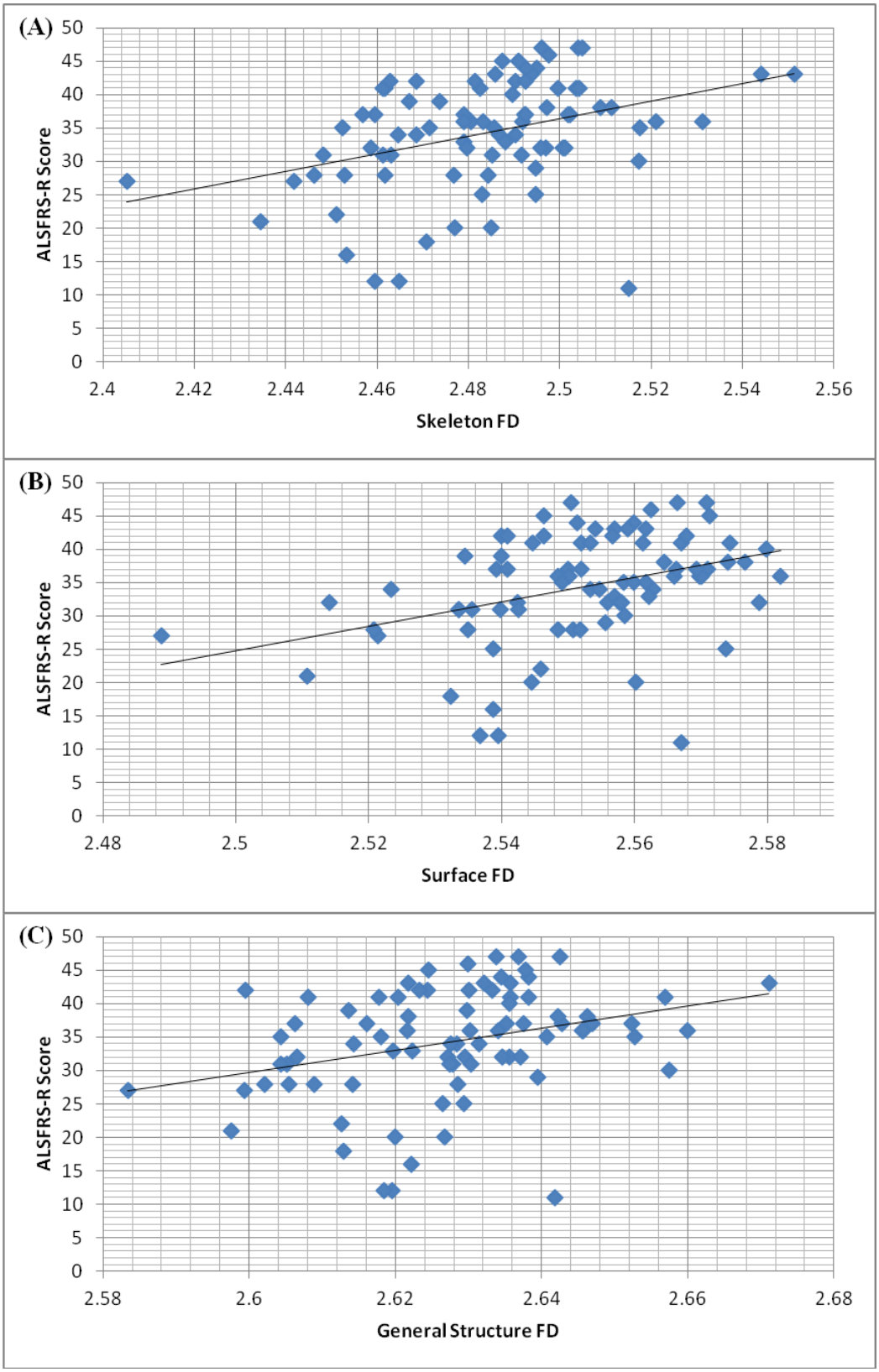

Figure 16: Correlation graphs showing Spearman's rank correlation coefficient (r_s) between ALSFRS-R scores and FDs of skeleton (A, r_s =0.42, *P*=0.0001), surface (B, r_s =0.40, *P*=0.0002), and general (C, r_s =0.38, *P*=0.0004).

The positive correlation between ALSFRS-R scores and the FDs indicates that ALS patients with better function status have a more complicated structure in all the interior, surface, and general shapes of brain WM structure. A positive correlation between the FA of the CST and ALSFRS-R score has been found to suggest that a low ALSFRS-R score reflects a loss of fiber connectivity and axonal degeneration (Thivard et al., 2007). A decrease in DTI FA (fractional anisotropy) would confirm a loss of fiber integrity by axonal degeneration. The data presented in this thesis finds the same conclusion.

4.4. Hemispheric Asymmetry in Brain WM of ALS Patients

The WM complexity asymmetry could be function-related and reflect influences from disease. In health people, the complexity of WM surface convolution was symmetrical between hemispheres and the complexity of the interior and general structures had a rightward asymmetry (Zhang et al., 2007). In this study, the data revealed that WM had leftward complexity asymmetry pattern in the interior (skeleton) structure of the ALS-FTD and the ALS-classic patients, suggesting that WM degeneration may be more severe in the right hemisphere than in the left hemisphere for those two subgroups.

The predominantly right-sided FTD patients (the FTD patients with predominantly right hemisphere degeneration) are marked with some behavioral alteration (e.g. poor impulse control, childish) (Mychack et al., 2001). The right hemisphere is dominant in both the comprehension and expression of emotion (e.g. speech intonation, body gesturing) (Tucker et al., 1995). In that case, the FTD patients, who suffer more damage on the right than the left hemisphere, may show deficits in the interpretation of facial expressions (Borod et al., 1985), bizarre expression of affect (Mychack et al., 2001) and other disabilities.

4.5 Limitations and Future Directions

The images used in this study were clinical evaluation images that were not acquired specifically for research purposes. Therefore, the quality of the images could have been better such as collected with a 3T scanner. Some of the control subjects were not true healthy controls and this might have affected the measured values of this group and results of comparisons with patient groups. Volumetric measurements of grey and white matter of the brain were not compared with FD results in the patient groups. Future studies should correct these limitations. In addition, future research should correlate FD measures of WM structure complexity with DTI evaluation of WM integrity to better understand mechanisms of WM degeneration in ALS. Longitudinal evaluations of brain grey and white matters and cognitive and sensorimotor functions of ALS patients would provide critical information for understanding the disease progression and for seeking effective treatments.

4.6 Conclusion

ALS patients with frontal-temporal lobe dementia have greatest brain white matter structural degeneration among ALS patients with different clinical signs. Grey matter loss in the frontal and temporal lobes could be the primary cause of the white matter degeneration in this category of patients. Brain WM structure is least affected in ALS patients with corticospinal tract hyperintensity signals among the classified ALS subgroups. This may be due to the fact that this group of patients experience the shortest ALS symptom duration. The level of WM structure degeneration in ALS is patient-type dependent. Fractal dimension measurement of the white matter structural complexity

correlates significantly with widely used clinical score of amyotrophic lateral sclerosis functional rating scale revised, suggesting that the structural measurement reflects functionality of the patients. Among the three forms of brain WM structure measured, skeleton is the most sensitive substructure for detecting WM structural degeneration in ALS patients. FD structural analysis in the whole brain was more sensitive than in a single hemisphere in detecting brain WM structural degeneration in ALS. Brain WM structure complexity is asymmetrical in ALS patients with dementia and ALS with an equal amount of upper and lower motor neuron signs.

4.7. Reference

Borod JC. Channels of emotional expression in patients with unilateral brain damage. Arch of Neurol 1985; 42:345-348.

Boxer AL. Clinical, neuroimaging and neuropathological features of a new chromosome 9p-linked FTD-ALS family. J Neurol Neurosurg Psychiatry 2011; 82:196-203.

Bregman BS. Recovery from spinal cord injury mediated by antibodies to neurite growth inhibitors. Nature 1995; 378:498-501.

GrandPre T. Nogo-66 receptor antagonist peptide promotes axonal regeneration. Nature 417: 547-551.

Hilliard MA. Axonal degeneration and regeneration: a mechanistic tug-of war. Journal of Neurochemistry 2009; 108:23-32.

Jokic N. The neurite outgrowth inhibitor Nogo-A promotes denervation in an amyotrophic lateral sclerosis model. EMBO Reports 2006; 7:1162-1167.

Karnezis T. The neurite outgrowth inhibitor Nogo A is involved in autoimmune-mediated demyelination. Nature Neuroscience 2004; 7:736-744.

Lee YC. MRI in ALS: corticospinal tract hyperintensity. Neurology 2003; 61:1600.

Mychack P. The influence of right frontotemporal dysfunction on social behavior in frontotemporal dementia. Neurology 2001; 56:S11-S15.

Prodan CI, Holland NR. Severe bilateral corticospinal tract degeneration in motor neuron disease. Journal of Clinical Neuromuscular Disease 2002; 3:183-184.

Rajagopalan V. Evaluation of upper motor neuron pathology in amyotrophic lateral sclerosis by MRI: towards indentifying noninvasive biomarkers of the disease, 2010.

Thivard L. Diffusion tensor imaging and voxel based morphometry study in amyotrophic

lateral sclerosis: relationships with motor disability. J Neurol Neurosurg Psychiatry 2007; 78: 889-892.

Tucker DM. Social and emotional self-regulation. Ann NY Acad Science 1995; 769:213-239.

Whitwell JL. Gray and white matter water diffusion in the syndromic variants of frontotemporal dementia. Neurology 2010; 74:1279-1287.

Yiu G, He Z. Glial inhibition of CNS axon regeneration. Neuroscience 2006; 7:617-627.

Zhang LD. Quantifying degeneration of white matter in normal aging using fractal dimension. Neurobiology of Aging 2007; 28:1543-1555.